



OPEN

Experimental study on the performance and mechanism of high-pressure abrasive water jet cutting GFRP bars reinforced concrete structures

Jingwei Xu^{1,3}, Hu Yu^{1,2,4}, Chuang Huang^{1,2,4}, Biao Li^{1,2}✉, Bin Liu^{1,2}, Jian Qiu³ & Jiwen Wang^{1,2}

Abrasive water jet (AWJ) cutting technology is considered an effective method to assist tunnel boring machines in efficiently breaking glass fiber reinforced polymer (GFRP) bar reinforced concrete structures. However, systematic investigations on the coupled cutting behavior of GFRP bars and concrete remain limited. To address this gap, this study presents the first comprehensive experimental analysis of AWJ cutting of GFRP-reinforced concrete, clarifying the removal mechanisms of both GFRP bars and concrete and revealing the key process parameters governing cutting depth. An innovative and systematic evaluation of AWJ process parameters was conducted by integrating single-factor experiments with orthogonal tests to elucidate the relative significance of each parameter on cutting depth. The results show that cutting GFRP bars with high-pressure AWJ can produce deeper cracks than cutting concrete. The cutting depth of GFRP bars and concrete is negatively correlated with traverse speed and standoff distance, and positively correlated with nozzle diameter, pump pressure, and number of cutting passes. When high-pressure AWJ cuts concrete, brittle fracture erosion is the main mechanism, resulting in smooth and flat cutting surfaces. The damage caused by pure water jet to concrete exhibits a water-wedge failure mode, propagating mainly along transitional weak interfaces and forming irregularly shaped failure surfaces. The relative importance of AWJ cutting parameters on concrete cutting depth is ranked as follows: traverse speed, number of cutting passes, standoff distance, pump pressure, and nozzle diameter. Recommended parameters for engineering applications include a pump pressure of 240 MPa, a traverse speed of ≤ 15 m/min, a standoff distance of approximately 40 mm, and a nozzle diameter of about 0.44 mm. Under these conditions, concrete can be cut with 2–3 passes and GFRP bars with a single pass, ensuring cutting efficiency while maintaining a balance among water consumption, equipment capacity, and construction safety. These findings extend the understanding of AWJ-assisted cutting of GFRP-reinforced concrete and provide theoretical guidance and practical references for jet-assisted rock breaking in Shield tunneling operations.

Keywords AWJ, GFRP concrete, Cutting performance, Damage mechanism

Shield tunneling method construction has the characteristics of high degree of automation, saving manpower, fast construction speed, and small environmental disturbance, and has become a key technology in transportation, mining, water conservancy and other engineering fields^{1–4}. The shield machine has become an indispensable and important equipment in the construction of subway tunnels and urban pipe corridors. During its excavation process, it can better adapt to a variety of stratigraphic conditions. However, it faces the complex and diverse urban underground environment, especially when encountering reinforced concrete will inevitably cause engineering problems such as steel bars wrapping around the cutterhead, damage to cutting tools, and low removal efficiency^{5–10}. Therefore, breaking down reinforced concrete obstacles such as underground diaphragm walls has become a new challenge for shield urban tunneling.

¹Geotechnical and Structural Engineering Research Center, Shandong University, No.17923 Jingshi Road, Jinan 250061, Shandong, China. ²School of Civil Engineering, Shandong University, Jinan, Shandong, China. ³Jinan Heavy Industries Group Co., Ltd, Jinan, Shandong, China. ⁴Hu Yu and Chuang Huang contributed equally to this work. ✉email: 717520670@qq.com

During the construction of tunnel projects, in order to further improve the shield machine's removal efficiency when encountering reinforced concrete obstacles, reduce tool wear, and prevent the screw machine from jamming, some scholars have proposed that GFRP bars can be used to replace the internal concrete steel bars^{11–13}. GFRP bars are a new type of composite material processed from a resin matrix and GFRP materials. GFRP bars offer several advantages, including excellent corrosion resistance, light weight, and outstanding durability under harsh environmental conditions. Their application not only enhances the structural performance and service life of concrete members but also reduces maintenance requirements^{14–17}. The typical manufacturing process is pultrusion, in which continuous glass fibers are thoroughly impregnated with a resin matrix, cured in a heated mold, and subsequently surface-treated to enhance bonding performance with concrete. Compared with traditional steel bars, they have higher tensile strength, lighter weight, and corrosion resistance. Therefore, they have been widely used in engineering^{18,19}.

With the gradual application of GFRP bars, GFRP bars reinforced concrete structures are used in corresponding parts such as the retaining piles, ground connection walls, and contact channel segment breaks that the tunnel boring machine will pass through, so that the tunnel boring machine can directly cut through, realizing the initial or arrival²⁰. However, during the application process, problems such as cutterhead and screw machine jamming were still encountered, resulting in low excavation efficiency. For example, when the shield machine of Shenyang Metro Lines 3 and 4 was grinding GFRP bars reinforcement piles, soil accumulation and screw failure occurred. The conveyor is stuck²¹. In order to explore the three-dimensional force characteristics and failure mechanism of the shield machine in breaking the GFRP bars reinforced concrete structure, the horizontal water jet mechanical cutter rock breaking test large scientific equipment independently developed by Shandong University was used to simulate the tunneling of glass fiber reinforced concrete. It was found that it would still, An equipment jam caused the test to be suspended. Therefore, there is an urgent need to develop a method that enables tunnel boring machines to efficiently penetrate concrete obstacles containing GFRP reinforcement.

In recent years, domestic and foreign scholars have conducted a large number of studies on high-pressure AWJs. Relevant studies have proven that water jet-assisted excavation of TBM, drill bits, picks, etc. has very good effects, can effectively reduce tool wear and significantly improve excavation efficiency^{22–28}, is considered to be a highly potential auxiliary excavation method. At the same time, high-pressure AWJs are widely used in other fields because of their high efficiency and environmental protection. In the field of metal processing, AWJs have shown significant advantages, and scholars have conducted a large number of studies. Sourd et al.²⁹ investigated the surface contamination and quality issues of titanium alloys after AWJ milling, followed by cleaning with a water jet. Based on the test results of abrasive jet cutting steel, Deepak et al.³⁰ pointed out that the jet standoff distance, abrasive particle size, nozzle diameter and incident angle have important effects on steel cutting. There is an optimal range for depth effects. Perec et al.³¹ conducted metal cutting experiments with abrasive jets and found that the metal cutting depth is positively related to the pump pressure and negatively related to the traverse speed. It first increases and then decreases as the abrasive supply increases. Brucely et al.³² explored the influence of jet parameters on metal cutting surface roughness and flick angle through experiments. Gnansasekaran et al.³³ systematically explored the effects of AWJ pressure, penetration rate, abrasive amount rate and nozzle distance on mixed metal. Effect of Erosion Rate of Fiber Laminates. In the field of concrete cutting, Liu et al.²⁵ used numerical methods to find that the abrasive concentration that optimizes the concrete crushing depth and damage efficiency is 20%. Hlaváček et al.³⁴ studied the influence of concrete age on the erosion effect of abrasive jets and found that one-year-old concrete was 28% more difficult to cut than new concrete. Xiao et al.³⁵ conducted numerical simulations of high-speed water jet impact on concrete based on the coupling algorithm of smooth particle hydrodynamics and finite element method, and studied the internal energy change rules and damage stress evolution of homogeneous and heterogeneous concrete in different times. law.

In addition, recent studies have further verified the potential applications of AWJ in the machining of composite and hybrid materials^{36,37}. For example, Sourd et al.³⁸ conducted a multiscale analysis of damage and contamination in abrasive water jet drilling of GLARE fiber-metal laminates, while Chaouch et al.³⁹ proposed a hybrid modeling and multi-objective optimization approach for AWJ machining of composite laminates based on neural networks and metaheuristic algorithms. These studies demonstrate that AWJ is also effective in cutting complex composite structures, thereby further extending the application potential of high-pressure AWJ beyond metal and concrete machining.

In summary, the aforementioned studies have fully demonstrated the superior capability of AWJ in cutting metals, concrete, and composite materials, highlighting their efficiency, precision, and controllability in processing complex structures. Accordingly, AWJ holds promise for pre-cutting GFRP-reinforced concrete obstacles to reduce the mechanical rock-breaking demand on tunnel boring machines, thereby enabling efficient advancement. Moreover, existing research indicates that the cutting depth of AWJ is a critical factor influencing the effectiveness of auxiliary mechanical rock-breaking, directly affecting cutter forces and rock-breaking efficiency. However, systematic studies on AWJ cutting of GFRP-reinforced concrete structures remain lacking, providing a clear direction for further exploration of AWJ-assisted high-efficiency tunneling.

In this study, cutting depth was adopted as the evaluation index to investigate the performance and mechanism of AWJ cutting of GFRP bars reinforced concrete. Five key parameters, including traverse speed, pump pressure, standoff distance, nozzle diameter, and number of passes, were examined through single-factor and orthogonal tests. The results demonstrated that AWJ can effectively cut GFRP bars reinforced concrete, with the main challenge lying in concrete removal. The mechanisms of GFRP bar and concrete removal under AWJ action were clarified, and the significance of control parameters affecting cutting depth was analyzed. By systematically addressing the coupled cutting behavior of both GFRP bars and concrete, this study extends the understanding of AWJ-assisted cutting and provides construction recommendations, offering theoretical guidance and technical references for AWJ-assisted tunnel boring machines.

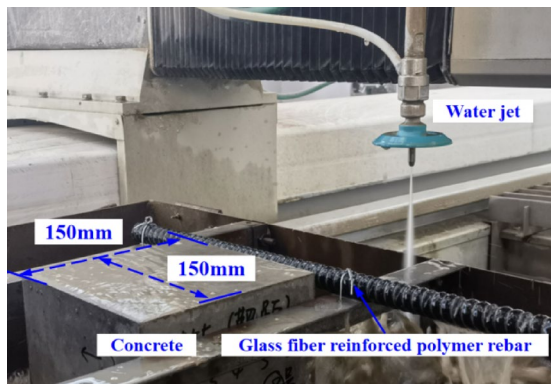


Fig. 1. Sample installation.

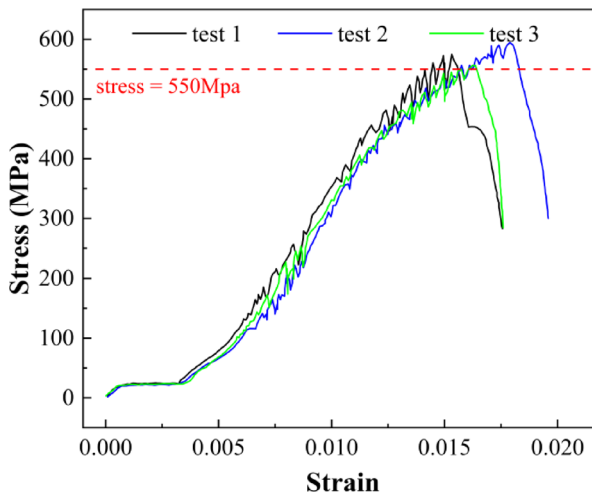


Fig. 2. Stress-strain curve of GFRP reinforcement.

Experimental designs

Experimental apparatus and rock sample parameters

This experimental study of high-pressure AWJ cutting of GFRP bars reinforced concrete was conducted on the multi-functional water jet cutting test platform of Shandong University. The test bench consists of high-pressure pump unit, numerical control console, abrasive tank, control system and other accessories. The high-pressure pump unit includes a supercharger, an intelligent cooling circulation system, etc. Six superchargers operating at the same time can achieve a maximum stable high-pressure water output of 420 MPa, which is the basis for supporting the continuous operation of the test platform. The water tank is connected to low-pressure water and provides sufficient water supply to the booster pump, which can achieve a maximum flow demand of 36 L/min. The water jet nozzle can be flexibly replaced with nozzles of different diameters to carry out efficient cutting tests. Through parameter settings, the numerical control console can run in the vertical direction of the nozzle to adjust the standoff distance for sample cutting. It can also run back and forth in two directions in the horizontal plane to complete water jet cutting tests under different traverse speed conditions. The abrasive tank provides a continuous supply of abrasives to the test platform. The negative pressure generated by the high-speed flow of high-pressure water at the water jet nozzle draws the abrasives into the high-pressure water through the hose, and is sprayed out with the high-pressure water. The control system integrates multiple functions such as pump unit starting, pressure adjustment, water valve switching and nozzle operating parameter setting, and is suitable for testing and parameter setting under various working conditions.

The materials used in this test were GFRP bars and concrete (Fig. 1). The GFRP bar has a diameter of 25 mm and a length of 500 mm. It is composed of approximately 60% glass fibers (by volume) and 40% epoxy resin matrix. The density of the GFRP bar is about 2.0 g/cm^3 , while the epoxy resin matrix has a density of 1.2 g/cm^3 and a tensile strength of 70 MPa. The GFRP bar exhibits a tensile strength greater than 550 MPa, a thermal expansion coefficient of 9.9, and a porosity of approximately 2%. Its stress-strain curve is shown in Fig. 2. The concrete strength grade is C35, and the test size is $200 \times 200 \times 150 \text{ mm}$. The mix proportions are listed in Table 1. After the specimen is produced, it is cured under constant temperature and humidity conditions for 28 days. The abrasive used in this experiment was commonly used natural garnet, characterized by high hardness and

Material type	Cementitious material	Fine aggregate		Coarse aggregate		Admixture	Water
Main component	Cement	Manufactured sand		Gravel		Pumping agent	/
Key technical index	/	Fineness modulus	3.2	Maximum size	25 mm	/	/
		Clay content	0.30%	Minimum size	5 mm		
		/	/	Gradation	continuous		
Weight ratio	1	1.71		2.26		0.05	0.39
Material dosage per m ³ (kg/m ³)	440	752		996		22.1	170

Table 1. Concrete composition and properties.

Level	Traverse speed m/min	Standoff distance cm	Pump pressure MPa	Nozzle diameter mm	Cutting times
1	2	2	150	0.36	1
2	4	4	200	0.44	2
3	6	6	240	0.50	3
4	8	8			
6	10	10			

Table 2. Single factor experimental factors and levels.

strength, with a Mohs hardness of 7–9, a density of 3.54 g/cm³, and a particle size of 80 mesh (ranging from 0.18 to 0.25 mm).

Experimental test procedure

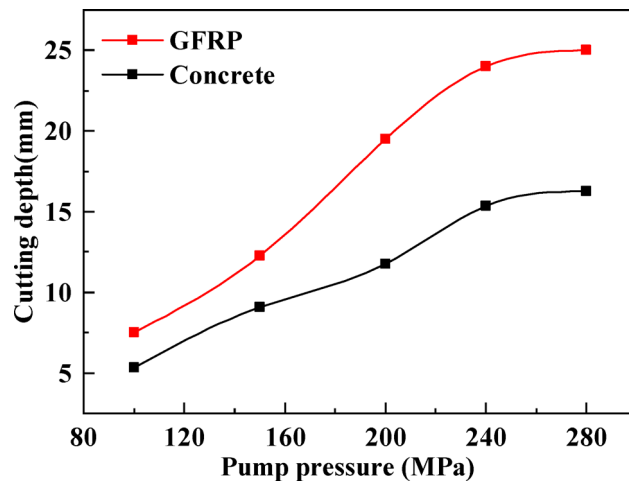
The effect of high-pressure AWJ cutting of GFRP bars reinforced concrete is affected by multiple cutting parameters. Through previous experiments and literature research, this experiment set five control parameters: traverse speed, pump pressure, standoff distance, nozzle diameter, and number of cutting times. Conduct experimental research on the performance and mechanism of high-pressure AWJ cutting of GFRP bars reinforced concrete. In order to more clearly explore the cutting effect of the jet, a cutting comparison test was conducted between plain concrete test blocks and GFRP bars under the same working conditions. This study used the control variable method to conduct a single-factor test, as shown in Table 2. In this study, the abrasive flow rate was set at a fixed value of 960 g/min. The ranges of traverse speed and standoff distance were primarily determined based on the operating conditions of the tunnel boring machine and the cutting capacity of the abrasive water jet. Typically, the cutterhead rotational speed of a shield machine ranges from 0.5 to 2 rpm, and traverse speeds of 2–10 m/min can accommodate all commonly used water nozzles. Considering the protective structures and corresponding safety measures for the cutterhead nozzles, the standoff distance should not be less than 2 cm to avoid nozzle damage or compromise experimental safety. The upper limit of 10 cm ensures effective jet coverage of the specimen surface while maintaining experimental flexibility. The selection of pump pressure, nozzle diameter, and cutting passes also considered the pump capacity and the ability of the abrasive water jet to cut GFRP-reinforced concrete. The levels of pump pressure were set at 150, 200, and 240 MPa; nozzle diameters at 0.36, 0.44, and 0.50 mm; and cutting passes at 1, 2, and 3. At the same time, a mixed orthogonal test with 5 factors and 5 levels was also designed to conduct a significance analysis on the influence of each parameter on the concrete cutting depth, as shown in Table 3.

The experimental procedure is described as follows. Prior to testing, the operating parameters were set and the nozzle was positioned to allow sufficient space for sample placement. The test block was then hoisted to the designated position, ensuring that one side was perpendicular to the cutting direction of the nozzle. Subsequently, the cutting parameters were configured, the pump unit was started, and the high-pressure water valve was opened. Once the system pressure stabilized, the abrasive valve was activated to perform the cutting. After completing a cut, the nozzle was repositioned to the next location, maintaining a 20 mm spacing between consecutive cuts. This procedure was repeated until all designated cuts were completed.

After each group of test blocks was cut, residual abrasives and concrete fragments in the cutting joints were rinsed with clean water and further cleaned using high-pressure air before air-drying. The depth of the slits was measured using a steel needle and a telescopic gauge, taking readings from both sides of the vernier scale. To ensure measurement accuracy, each slit was assessed at five equally spaced points and the average value was calculated.

In addition, the surface failure patterns of the concrete and GFRP bars were visually inspected and documented with photographs throughout the experiment, enabling a comprehensive analysis of the failure mechanisms.

Level	Traverse speed m/min	Standoff distance cm	Pump pressure MPa	Nozzle diameter mm	Cutting times	Depth of cutting mm
1	2	2	150	0.36	3	18.92
2	2	4	200	0.44	6	19.42
3	2	6	240	0.5	9	13.08
4	2	8	150	0.36	3	9.42
5	2	10	240	0.5	9	11.17
6	4	2	200	0.5	8	13.67
7	4	4	240	0.36	9	7.00
8	4	6	150	0.5	3	10.17
9	4	8	240	0.36	6	9.42
10	4	10	150	0.44	9	3.92
11	6	2	240	0.5	6	12.00
12	6	4	150	0.36	9	4.00
13	6	6	240	0.44	3	8.17
14	6	8	150	0.5	9	3.67
15	6	10	200	0.36	3	7.17
16	8	2	150	0.44	9	3.83
17	8	4	240	0.5	3	11.00
18	8	6	150	0.36	6	4.17
19	8	8	200	0.5	9	4.08
20	8	10	240	0.36	3	5.83
21	10	2	240	0.36	9	4.00
22	10	4	150	0.5	3	4.42
23	10	6	200	0.36	9	2.75
24	10	8	240	0.44	3	7.33
25	10	10	150	0.5	6	3.92

Table 3. Orthogonal test scheme and result.**Fig. 3.** Effect of the pump pressure on cutting depth.

Results analysis

Influence of pump pressure parameters on cutting performance

Pump pressure is one of the key factors affecting the jet slit depth. Historically, when water jets were first applied in the cutting field, pump pressure was regarded as the fundamental parameter governing cutting performance, which also directly promoted the development of large-capacity high-pressure plunger pumps and boosters.

Figure 3 presents the influence of pump pressure on the cutting depth when high-pressure AWJ is used to cut GFRP bars and concrete specimens. It can be observed that, when other control parameters remain constant, increasing the pump pressure within a certain range has a pronounced effect on the jet cutting performance. This

is because a higher pump pressure results in a higher jet velocity, which enhances the kinetic energy transferred to the target material and accelerates the erosion and removal of material from the cutting surface.

Overall, AWJ cutting of GFRP bars achieves better performance compared with concrete under the same pump pressure. This difference arises because GFRP has a relatively lower density and heterogeneous fiber-matrix interface structure, making it more susceptible to erosion and fiber pull-out under jet impact, while concrete, with its dense aggregate-cement matrix, exhibits stronger resistance to material removal.

In the pressure range below 240 MPa, the cutting depth of GFRP bars increases almost linearly with pump pressure and consistently exceeds that of concrete. However, when the pump pressure increases from 240 MPa to 280 MPa, an inflection point appears in the curve: the cutting depth shows only a slight increase despite the 40 MPa pressure increment. This trend indicates that, beyond a certain threshold, jet energy utilization becomes less efficient due to increased jet dispersion, energy loss in turbulence, and partial saturation of the erosion process at the cutting front.

Therefore, in practical engineering applications, it is recommended to maintain the pump pressure around 240 MPa, as further increases yield limited improvements in cutting depth while significantly raising energy consumption and equipment wear. This optimal balance point ensures both effective cutting performance and economic feasibility during shield tunneling operations involving reinforced concrete obstacles.

Influence of traverse speed on cutting performance

During the AWJ cutting process, changes in traverse speed have a significant impact on the cutting performance. As shown in Fig. 4, as the traverse speed increases, the cutting depth of both GFRP bars and concrete initially decreases rapidly and then decreases more slowly. This trend is consistent with the parameter effects observed by Thakur et al.^{40–46} in CFRP composites, indicating that AWJ cutting efficiency is strongly influenced by traverse speed.

When the traverse speed is 0.5 m/min, the concrete cutting depth reaches 35.2 mm, and the GFRP bars are completely severed. At a traverse speed of 1 m/min, the cutting depth of the concrete is 20.6 mm, and that of the GFRP bars is 24 mm. With further increase of the traverse speed, the cutting depth of the GFRP bars consistently exceeds that of the concrete, especially in the range of 2–15 m/min. This difference arises because GFRP has a relatively lower density and weaker fiber-matrix interfaces, making it more susceptible to jet erosion, whereas concrete, with its denser aggregate-cement matrix, provides stronger resistance to material removal.

When the traverse speed exceeds 15 m/min, the cutting depth of concrete falls below 5 mm, and the cutting effect becomes minimal, suggesting that the jet energy cannot fully act on the material due to the reduced interaction time. This observation emphasizes the importance of balancing traverse speed to achieve both cutting efficiency and operational efficiency.

Therefore, in practical engineering applications, it is recommended to control the jet traverse speed within 15 m/min to ensure effective cutting performance. Maintaining a moderate traverse speed allows sufficient jet exposure time to the target material, maximizes material removal, and ensures consistent cutting quality for both GFRP bars and reinforced concrete structures.

Influence of standoff distance on cutting performance

The standoff distance is defined as the distance between the AWJ nozzle and the surface of the material to be cut. Figure 5 illustrates how cutting depth varies with standoff distance. As the distance between the jet nozzle and the target surface increases, the discreteness of the jet beam becomes larger, leading to a deterioration in cutting performance.

For GFRP bars, the cutting depth exhibits a linear negative correlation with standoff distance: within the range tested, smaller standoff distances result in better cutting performance. This is because GFRP bars are cylindrical and have lower density and hardness than concrete. When the standoff distance is small, the jet can

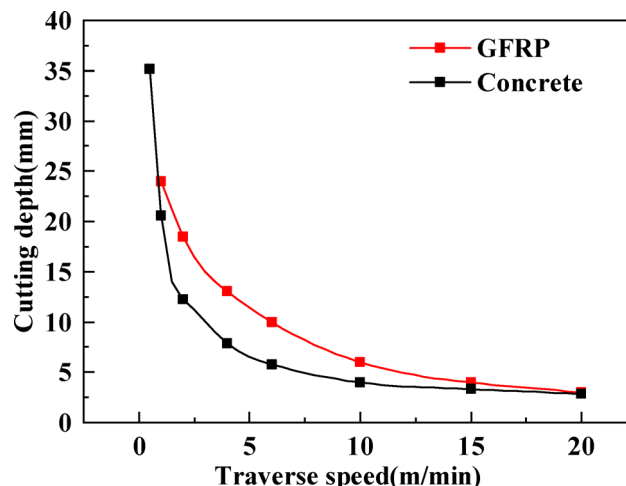


Fig. 4. Effect of the traverse speed on cutting depth.

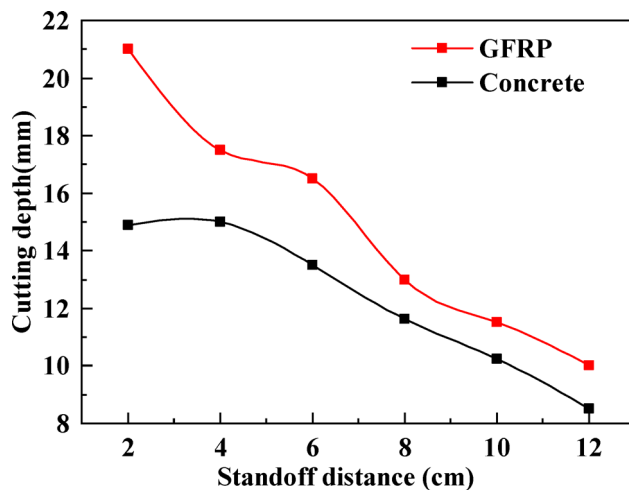


Fig. 5. Effect of the standoff distance on cutting depth.

fully act on the edge of the GFRP bar with minimal reflection, enhancing material removal. The initial cutting distance is effectively greater than the set standoff distance due to the cylindrical shape, and the reflected jets are fewer, further promoting cutting efficiency.

For concrete, the trend is more complex. When the standoff distance is less than 40 mm, the cutting depth increases slightly with increasing distance. This is likely due to the interaction between the jet and the groove formed during initial cutting, which improves jet penetration. When the standoff distance exceeds 40 mm, the cutting depth decreases sharply in an approximately linear manner. In this case, increased distance leads to jet dispersion and energy loss, reducing the effective erosion on the concrete surface. Therefore, an optimal standoff distance exists for AWJ cutting of concrete to maximize cutting depth; in this study, the optimal distance is 40 mm.

The differences between GFRP bars and concrete can be attributed to their material properties and geometry. Concrete grooves constrain the jet and produce reverse vertical jets, which weaken cutting efficiency, whereas GFRP bars do not exhibit this phenomenon. Moreover, GFRP bars' lower density and hardness facilitate cutting even at slightly larger standoff distances.

From an engineering perspective, since concrete is more difficult to cut, practical applications mainly consider the optimal standoff distance for concrete. Therefore, it is recommended to set the standoff distance around 40 mm to achieve the best cutting effect in reinforced concrete structures while maintaining effective cutting of GFRP bars.

Influence of nozzle diameter on cutting performance

The nozzle diameter directly reflects the flow rate of the abrasive water jet. Under a fixed pump pressure, a larger nozzle diameter results in a higher flow rate, which increases the kinetic energy delivered to the target material and improves the cutting performance. In this study, tests were conducted using nozzles of four different diameters, as shown in Fig. 6.

The results indicate that as the nozzle diameter increases, the difference in cutting depth between GFRP bars and concrete becomes more pronounced. When the nozzle diameter is 0.25 mm, the cutting depths for GFRP bars and concrete are approximately 7 mm and 7.5 mm, respectively, showing minimal difference. As the nozzle diameter increases, the cutting depth initially rises rapidly and then increases more gradually. When the nozzle diameter exceeds 0.44 mm, although the water flow rate and consumption increase significantly, the improvement in cutting depth becomes negligible, indicating that the cutting efficiency approaches a saturation point.

This behavior can be explained by the jet energy transfer mechanism. At small nozzle diameters, the flow rate is limited, resulting in lower jet momentum and energy density, and thus slower material removal. As the diameter increases, the flow rate and jet impact area increase, enhancing the material removal capacity. However, beyond a certain diameter, the jet energy becomes more dispersed over the larger nozzle exit area, and the unit-area impact energy does not significantly increase, which limits further improvement in cutting depth.

From a practical engineering perspective, to maximize cutting efficiency while minimizing excessive water consumption, it is recommended to select a nozzle diameter of approximately 0.44 mm. This choice provides an optimal balance between effective cutting performance and operational cost in AWJ-assisted cutting of GFRP-reinforced concrete structures.

Influence of cutting times on cutting performance

In addition to varying the control parameters, performing multiple cutting passes on the same target can also enhance the cutting effect when using AWJ to cut GFRP bars and concrete. As shown in Fig. 7, considering that the diameter of the GFRP bar is only 25 mm, it can be completely severed by a single pass of the AWJ. To ensure

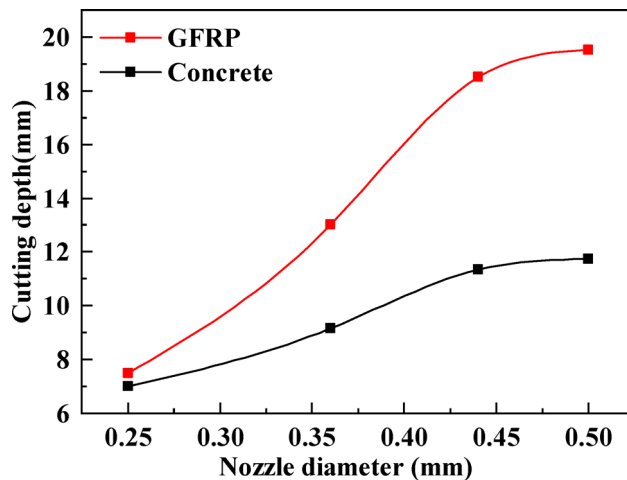


Fig. 6. Effect of the nozzle diameter on cutting depth.

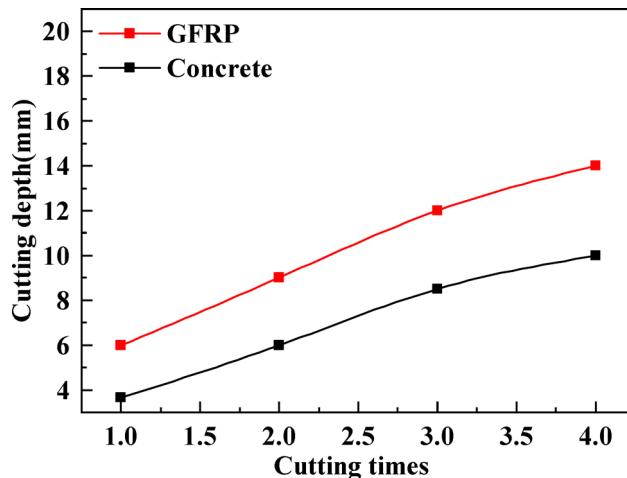


Fig. 7. Effect of the cutting times on cutting depth.

the regularity and comparability of multiple cuts, the traverse speed was adjusted from 2 m/min to 10 m/min, and both GFRP bars and concrete were subjected to four consecutive cutting passes.

The results indicate that, overall, within the first three passes, there is an approximately linear positive correlation between the slit depth and the number of cutting passes. At the fourth pass, however, the slope of the curve decreases, indicating that as the slit depth increases, the effective standoff distance for the subsequent cutting passes becomes larger. Consequently, the material removal effect of a single jet pass gradually weakens.

This trend can be explained by the interaction between the jet and the growing slit. Initially, the jet acts directly on the material surface, providing maximum impact energy and material removal. As the slit deepens, part of the jet energy is lost due to increased distance and jet dispersion within the slit, reducing the efficiency of additional passes.

From a practical engineering perspective, the cutting effect of the jet under high traverse speed can be improved by appropriately increasing the number of cutting passes. Optimizing the number of passes allows the jet to remove material more effectively, ensuring sufficient cutting depth for both GFRP bars and reinforced concrete structures without excessively slowing down the overall operation.

Discussion

Mechanism analysis

Figure 8 shows the macroscopic fracture characteristics of concrete cut by high-pressure pure water jet and high-pressure AWJ under different standoff distance conditions. The results show that there are significant differences in the groove shapes of concrete specimens under the action of the two jets. The damage range on both sides of the slit formed by AWJ cutting of concrete is roughly symmetrically distributed, and the wall surface of the slit is relatively smooth. However, the concrete under the action of high-pressure pure water jets formed abnormal grooves with irregular and rough contours. The lengths and expansion directions of cracks on both sides of the

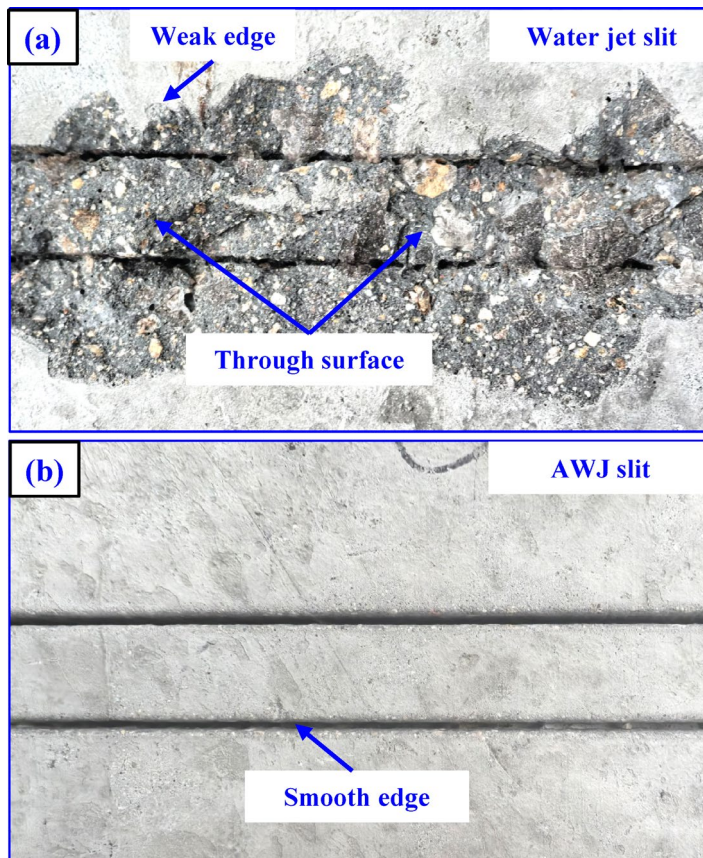


Fig. 8. Macro fracture characteristics of concrete.

grooves were different and asymmetrical. The above phenomenon is mainly caused by the difference in concrete structure and the different mechanism of water jet rock breaking.

Concrete is a reliable heterogeneous structural material with significant differences in the strength and density of the mortars and aggregates in its composition. Under the action of high-pressure pure water jet, due to the high porosity and abundant micro-cracks at the transition interface between aggregate and cement mortar, it leads to the preferential orientation of crack propagation. Internal cracks in concrete preferentially expand along the interface between aggregate and mortar. This interface is a weak connection zone and the bonding strength is relatively weak. When a weak interface is encountered, cracks that partially penetrate the aggregate will further propagate along the interface between the aggregate and the mortar under the impact force induced by the high-speed jet. The water wedge effect of the water jet can be fully utilized at the above-mentioned transition interface, which is the preferred area for high-pressure water jets to penetrate concrete and the preferred area for crack initiation and expansion. Therefore, the fracture cracks of concrete under the action of high-pressure pure water jet are asymmetrically distributed and mainly expand along the transitional weak connection interface, thus forming an irregularly shaped failure surface.

The high-pressure AWJ cuts the concrete more regularly. The reason is the energy transfer of the jet beam. The erosion ability of the abrasive jet on the concrete mainly depends on the contribution of the abrasive particles. With the addition of abrasive particles, part of the kinetic energy of the water body is converted into the kinetic energy of the abrasive particles, resulting in a reduction in the water wedge effect of the jet, strengthening the grinding ability of the abrasive particles, and greatly improving the erosion ability of the water jet. The damage caused by abrasive particles to concrete is divided into brittle fracture erosion and plastic shear erosion. Brittle fracture erosion causes the cracks in the concrete to continue to expand mainly along the original erosion cracks in the vertical direction. The crack length and damage gradually increase as the standoff distance decreases. Increases, but the crack shape and expansion path remain unchanged, and plastic shear erosion makes the concrete incision flatter and smoother.

Figure 9(a) shows the slits on GFRP bars cut by both pure water jet and high-pressure AWJ. The slit produced by AWJ is about three times wider than that produced by the pure water jet. Figure 9(b) presents the cross-section of the GFRP bars cut by the pure water jet, showing noticeable scratches. In contrast, the cross-section cut by AWJ (Fig. 9(c)) is much smoother.

Compared with concrete, fiberglass bars are homogeneous materials. At the same time, the pure water jet has strong cutting ability only at the center of the jet, so the incision is narrow and smooth. The entire jet beam of the AWJ is filled with abrasive particles, and the edge of the jet beam still has strong cutting ability, which can abrade the incision at the opening. Large, forming a V-shaped incision. Therefore, the notches eroded by abrasive jets

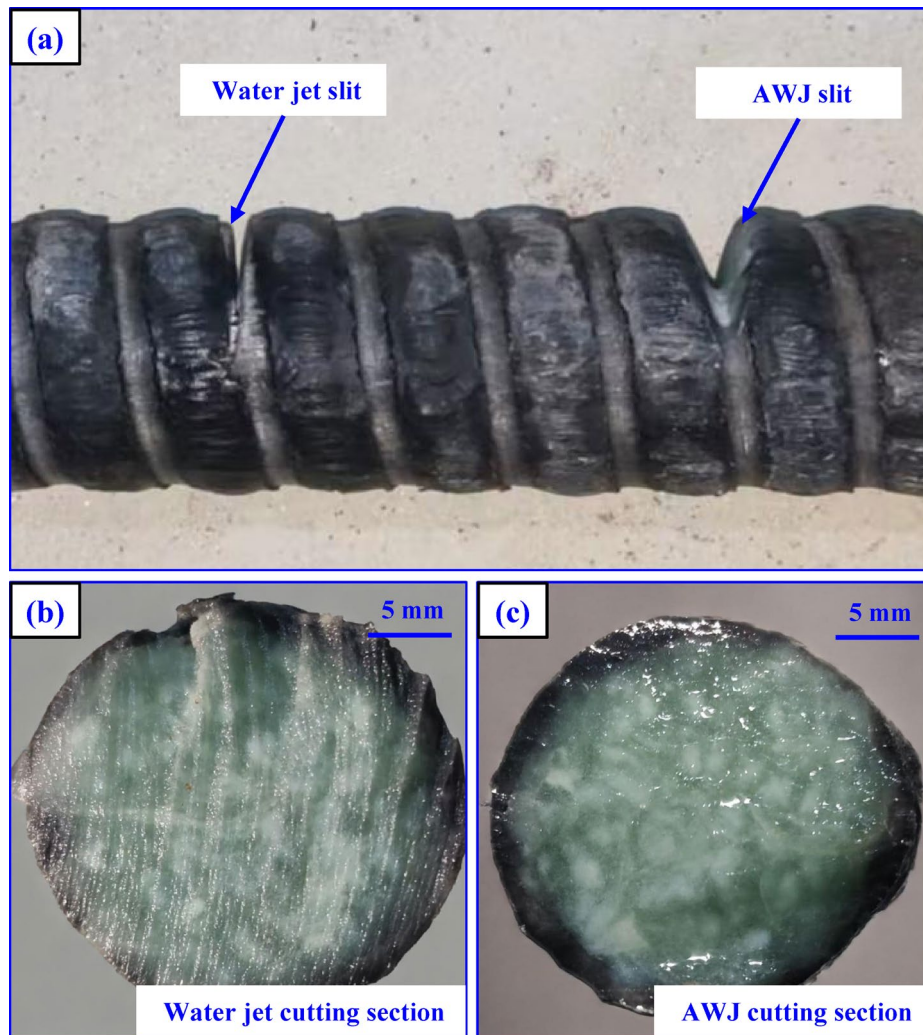


Fig. 9. Macro fracture characteristics of GFRP bars.

are larger than those eroded by pure water jets. This phenomenon is opposite to the macroscopic phenomenon of concrete slits. The damage to GFRP bars caused by pure water jets and AWJs is mainly plastic shear damage.

Scanning electron microscopy was performed on the cross-sections of GFRP bars after AWJ cutting, revealing distinct layering characteristics, as shown in Fig. 10. The fracture morphology varies from top to bottom: in the upper region, the glass fiber cross-sections remain intact, with smaller fiber diameters and relatively smooth surfaces, as shown in Fig. 10(b); in the middle region, the fiber diameters gradually increase and exhibit nearly elliptical cross-sections with more pronounced cutting marks, as shown in Fig. 10(c); in the lower region, the fiber cross-sections are irregular, with larger diameters and some residual fiber lengths, as shown in Fig. 10(d). This is attributed to the significant reduction in the velocity and kinetic energy of abrasive particles in the lower portion of the jet, which limits brittle fracture of the glass fibers, causing bending and tensile deformation during cutting and resulting in irregular plastic fracture surfaces. These observations indicate that the AWJ cutting mechanism of GFRP bars involves not only the impact and abrasion by high-speed abrasive particles but also bending–tensile failure of fibers, leading to a progressive evolution of the cross-sectional morphology from intact to coarse to irregular from top to bottom.

Significance analysis of cutting depth of concrete on AWJ parameters

In order to clarify the significance of the key parameters of water jet when cutting GFRP bars reinforced concrete structures with AWJ, the optimal parameter optimization sequence can be achieved to achieve efficient cutting in actual projects. Based on the previous single-factor experiment, a comparative experimental study on the cutting depth of GFRP bars and concrete cut by AWJ was conducted, and it was found that the cutting effect is affected by multiple cutting parameters. This is contrary to the results of Wang et al.⁴⁷ regarding abrasive water jet cutting of reinforced concrete. Since cutting concrete with AWJ is more difficult than cutting fiberglass bars, only concrete was considered when considering the significance study of control parameters. In order to explore the influence of each parameter on concrete cutting depth, variance analysis was performed on the orthogonal test data in Table 2. The analysis results are shown in Table 4. By analyzing the F value in the table, the significance of

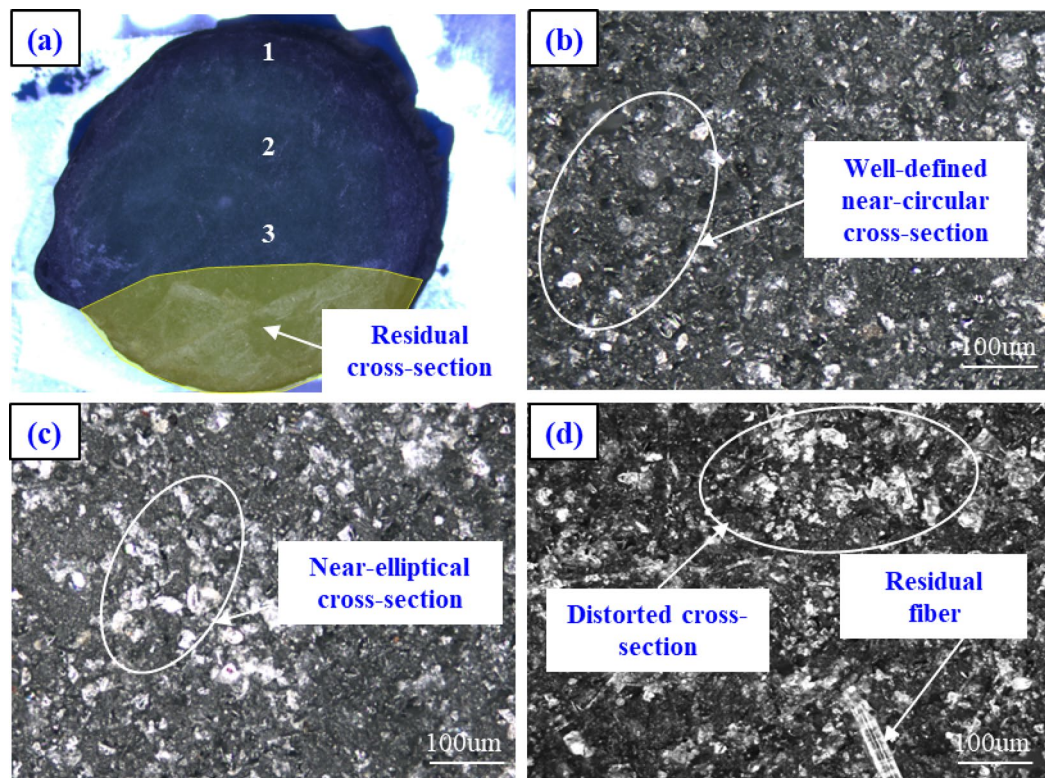


Fig. 10. Scanned image of GFRP bars.

Factor	S_j	Degrees of freedom	$S_j/\text{Degrees of freedom}$	F	Critical value	Significance
Traverse speed	299.4	4	74.9	89.09	$F_{0.05}(4,24)=2.78$	Significant
Cutting times	103.8	2	51.9	61.747	$F_{0.05}(4,24)=3.40$	Significant
Standoff distance	58.1	4	14.5	17.30	$F_{0.05}(4,24)=2.78$	Significant
Pump pressure	36.3	2	18.2	21.62	$F_{0.05}(2,24)=3.40$	Significant
Nozzle diameter	11.7	2	5.8	6.95	$F_{0.05}(2,24)=3.40$	Significant
Empty column	3.6	4	0.9	1.07	$F_{0.05}(4,24)=2.78$	
Error	16.8	6	0.8			

Table 4. Significance evaluation of each factor.

each parameter is ranked: traverse speed, cutting times, standoff distance, pump pressure, and nozzle diameter. This is consistent with the results of Karakurt et al.⁴⁸ Among them, the effect of traverse speed is much higher than that of other factors, followed by the number of cutting times. The F values of both are significantly greater than other influencing factors. For shield AWJ cutting of reinforced concrete, the traverse speed, cutting times and conventional cutting conditions are significantly different, and these two factors have the greatest impact on the depth of concrete cutting seams and need to be focused on.

Recommendation

Through this single-factor experimental study, it was found that the cutting depths of GFRP bars and concrete cut by AWJs are quite different. Under the same control parameters, the cutting depth of GFRP bars is much greater than the cutting depth of concrete. Therefore, when applying AWJ cutting in engineering, the main thing to consider is the cutting effect of concrete. In actual construction, considering the cutting effect, it is recommended to control the pump pressure at 240 MPa and the jet traverse speed within 15 m/min. It is recommended to give priority to a nozzle with a diameter of 0.44 mm. The order of importance of jet control parameters obtained through orthogonal experiments is traversing speed, cutting times, standoff distance, pump pressure, and nozzle diameter.

Therefore, during the construction process, after the pump pressure reaches a certain value, continuing to increase will have little impact on the rock breaking effect, but the requirements for equipment will be greatly increased and the safety risks of construction will be increased. Therefore, it is recommended that the pump pressure be 240 MPa, which is more appropriate. It can maximize the capabilities of the equipment and

reduce costs. The selection of the nozzle diameter is also very important in construction. To achieve efficiency enhancement when a shield machine is equipped with a water jet, multiple water jet nozzles need to work at the same time to achieve an obvious promotion effect. Multiple nozzles mean higher requirements for the total flow rate of the equipment. Blindly pursuing large flow rates will require a large enough energy storage space, which is difficult to achieve in the limited space of the tunnel. Therefore, choosing a suitable nozzle diameter is conducive to the successful implementation of the equipment. For application, it is recommended to make reasonable nozzle selection based on the layout of the water jet. At the same time, it is concluded from orthogonal experiments that the traverse speed has the greatest impact on the jet cutting effect, followed by the cutting times. Therefore, the optimal cutting depth can be achieved by reducing the cutting speed or performing multiple cuts.

Conclusions

This study systematically investigated the kerf depth and cutting mechanism of high-pressure AWJ cutting of GFRP bars and concrete, clarified the effects of key jet parameters, and identified the optimal range for efficient cutting. The significance of each control parameter was analyzed through orthogonal experiments. The main conclusions are as follows:

- (1) The cutting depth of high-pressure AWJ on GFRP bars is greater than that on concrete. The cutting depth of both GFRP bars and concrete is negatively correlated with traverse speed and standoff distance, and positively correlated with nozzle diameter, pump pressure, and number of cutting passes.
- (2) Concrete cutting is primarily governed by brittle fracture and plastic shear erosion, resulting in smooth kerf surfaces. In contrast, pure water jet cutting of concrete produces water-wedge damage, with cracks propagating along weak interfaces and forming irregular surfaces. GFRP bars, due to their low density and weak fiber-matrix interface, are more easily cut.
- (3) Variance analysis indicates that traverse speed has the greatest influence, followed by the number of cutting passes, standoff distance, pump pressure, and nozzle diameter. F-values show that traverse speed and the number of passes are the dominant factors, whereas increasing pump pressure beyond 240 MPa or using a larger nozzle diameter has limited effect on cutting depth.
- (4) For engineering applications, the recommended parameters are a pump pressure of 240 MPa, traverse speed ≤ 15 m/min, standoff distance of approximately 40 mm, and nozzle diameter of about 0.44 mm, with 2–3 passes for concrete and a single pass for GFRP bars. These parameters ensure cutting efficiency while balancing water consumption, equipment capacity, and construction safety.

Data availability

The datasets used and/or analysed during the current study are available from the corresponding author on reasonable request.

Received: 26 February 2025; Accepted: 31 October 2025

Published online: 28 November 2025

References

1. Di, Q. G., Li, P. F., Zhang, M. J. & Cui, X. P. Experimental study of face stability for shield tunnels in sandy cobble strata of different densities. *Tunn. Undergr. Space Technol.* **135**, 105029 (2023).
2. Maeda, M. & Kushiyama, K. Use of compact shield tunneling method in urban underground construction. *Tunn. Undergr. Sp Technol.* **20**, 159–166 (2005).
3. Wu, H., Shen, S., Liao, S. & Yin, Z. Longitudinal structural modelling of shield tunnels considering shearing dislocation between segmental rings. *Tunn. Undergr. Space Technol.* **50**, 317–323 (2015).
4. Zhang, W. et al. Soft computing approach for prediction of surface settlement induced by Earth pressure balance shield tunneling. *Undergr. Space.* **6**, 353–363 (2020).
5. He, S. et al. Pile group response induced by adjacent shield tunnelling in clay: scale model test and numerical simulation. *Tunn. Undergr. Space Technol.* **120**, 104039 (2021).
6. Huang, K. et al. Three-dimensional displacement characteristics of adjacent pile induced by shield tunneling under influence of multiple factors. *J. Cent. South. Univ.* **29**, 1597–1615 (2022).
7. Liu, C., Zhang, Z. & Regueiro, R. A. Pile and pile group response to tunnelling using a large diameter slurry shield – Case study in Shanghai. *Comput. Geotech.* **59**, 21–43 (2014).
8. Li, Z., Chen, Z., Wang, L., Zeng, Z. & Gu, D. Numerical simulation and analysis of the pile underpinning technology used in shield tunnel crossings on Bridge pile foundations. *Undergr. Space.* **6**, 396–408 (2021).
9. Xu, Q. et al. A case history of shield tunnel crossing through group pile foundation of a road Bridge with pile underpinning technologies in Shanghai. *Tunn. Undergr. Sp Technol.* **45**, 20–33 (2015).
10. Yan, L., Wang, G., Chen, M., Yue, K. & Li, Q. Experimental and application study on underpinning engineering of bridge pile foundation. *Adv. Civ. Eng.* **2018**, 1–13 (2018).
11. Bujotzek, L., Apostolidi, E. & Waldmann, D. Novel model for the determination of stress redistribution in GFRP reinforced concrete members under long-term Compressive Sion based on experimental results. *Constr. Build. Mater.* **432**, 136619 (2024).
12. Shan, Z., Liang, K. & Chen, L. Bond behavior of helically wound FRP bars with different surface characteristics in fiber-reinforced concrete. *J. Build.* **65**, 105504 (2023).
13. Wang, Z., Li, Z., Yang, J. Q., Huang, F. & Feng, P. Axial compressive and seismic performance of GFRP wrapped square RC columns with different scales. *J. Build.* **62**, 105342 (2022).
14. Aydin, F., Akyürek, M., Arslan, S. & Yilmaz, K. Effects of concrete cover thickness and concrete strength on temperature transfer in high-temperature exposed FRP reinforced concrete. *Rev. Constr.* **22**, 242–258 (2023).
15. Aydin, F. Experimental study on the flexural behaviour of a novel concrete-filled hybrid beams reinforced with GFRP and steel bars. *KSCE J. Civ. Eng.* **23**, 4710–4717 (2019).
16. Aydin, F. et al. Experimental investigation of the effects of FRP bar fiber type and surface characteristics on the performance of reinforced concrete beams. *Iran. J. Sci. Technol. Trans. Civ. Eng.* **48**, 1903–1915 (2024).

17. Aydin, F. et al. An experimental investigation of flexural performance of FRP reinforced concrete slabs. *Int. J. Civ. Eng.* **22**, 2269–2282 (2024).
18. Ozbakkaloglu, T. & Saatcioglu, M. Seismic performance of square high-strength concrete columns in FRP stay-in-place formwork. *J. Struct.* **133**, 44–56 (2007).
19. Zeng, J. J., Duan, Z. J., Gao, W. Y., Bai, Y. L. & Ouyang, L. J. Compressive behavior of FRP-wrapped seawater sea-sand concrete with a square cross-section. *Constr. Build. Mater.* **262**, 120881 (2020).
20. Hosseini, S. M., Mousa, S., Mohamed, H. M., Ferrier, E. & Benmokrane, B. Experimental and analytical investigation of precast fiber-reinforced concrete (FRC) tunnel lining segments reinforced with glass-FRP bars. *Tunn. Undergr. Sp Technol.* **139**, 105230 (2023).
21. Zhang, S. M. A brief analysis of the construction technology of shield tunneling through glass fiber reinforcement piles. *Construction mechanization.* **44**, 21–23 (2023).
22. Ciccu, R. & Grossi, B. Improvement of the excavation performance of PCD drag tools by water jet assistance. *Rock. Mech. Rock. Eng.* **43**, 465–474 (2010).
23. Gostimirovic, M., Pucovsky, V., Sekulic, M. & Rodic, D. Pejic. Evolutionary optimization of jet lag in the abrasive water jet machining. *Int. J. Adv. Manuf. Technol.* **101**, 3131–3141 (2019).
24. Lu, Y., Tang, J., Ge, Z., Xia, B. & Liu, Y. Hard rock drilling technique with abrasive water jet assistance. *Int. J. Rock. Mech. Min. Sci.* **60**, 47–56 (2013).
25. Liu, X., Tang, P., Geng, Q. & Wang, X. Effect of abrasive concentration on impact performance of abrasive water jet crushing concrete. *Shock Vib.* **2019**, 3285150.1–3285150.18 (2019).
26. Liu, S. et al. Experimental investigation of hard rock breaking using a conical pick assisted by abrasive water jet. *Rock. Mech. Rock. Eng.* **53**, 4221–4230 (2020).
27. Li, B. et al. Full-scale linear cutting tests to study the influence of pre-groove depth on rock-cutting performance by TBM disc cutter. *Tunn. Undergr. Sp Technol.* **122**, 104366 (2022).
28. Pan, Y., Liu, Q., Liu, J., Liu, Q. & Kong, X. Full-scale linear cutting tests in Chongqing sandstone to study the influence of confining stress on rock cutting efficiency by TBM disc cutter. *Tunn. Undergr. Sp Technol.* **80**, 197–210 (2018).
29. Sourd, X. et al. Plain water jet cleaning of titanium alloy after abrasive water jet milling: surface contamination and quality analysis in the context of maintenance. *Wear* **477**, 20383 (2021).
30. Deepak, D., Akash, V. & Anjaiah, D. Studies on jet penetration and Kerf width at various operating pressure in machining of D2 heat treated steel using abrasive water jet. *Int. J. Res. Eng. Technol.* **4** (9), 344–347 (2015).
31. Perec, A. Experimental research into alternative abrasive material for the abrasive water-jet cutting of titanium. *Int. J. Adv. Manuf. Tech.* **97**, 1529–1540 (2018).
32. Brucely, Y., Aultrin, J., Jaison, D. & K. S., & Using genetic algorithm optimizing the cutting parameters of AWJM process for aluminium 6061 alloy. *Int. J. Recent. Trends Eng. Res.* **5**, 48–56 (2019).
33. Gnansakaran, K., Rajesh, M. & Hariram, V. A study of abrasive water jet performance on hybrid metal fiber laminate. *Mater. Today: Proc.* (2024).
34. Hlaváček, P. et al. Influence of Concrete Age on Resistance to Fast Flowing Liquids. International Conference of Water Jet. Advances in Water Jetting. **2019**, 73–80 (2021).
35. Xiao, S. Q. et al. Damage and fracture characteristics of rocks with different structures under high-velocity water jet impact. *Eng. Fract. Mech. Volume.* **256**, 107961 (2024).
36. Thakur, R. K. & Singh, K. K. Abrasive waterjet machining of fiber-reinforced composites: A state-of-the-art review. *J. Braz Soc. Mech. Sci. Eng.* **42**, 381 (2020).
37. Thakur, R. K. & Singh, K. K. Evaluation of advanced machining processes performance on filler-loaded polymeric composites: A state-of-the-art review. *J. Braz Soc. Mech. Sci. Eng.* **43**, 300 (2021).
38. Sourd, X. et al. Multi-scale analysis of the damage and contamination in abrasive water jet drilling of GLARE fibre metal laminates. *J. Manuf. Process.* **84**, 610–621 (2022).
39. Chaouch, F. et al. Modeling and multi-objective optimization of abrasive water jet machining process of composite laminates using a hybrid approach based on neural networks and metaheuristic algorithm. *Proc. Inst. Mech. Eng. B J. Eng. Manuf. Ahead of Print*, (2024).
40. Thakur, R. K., Singh, K. K. & Ramkumar, J. Delamination analysis and hole quality of hybrid FRP composite using abrasive water jet machining. *Mater. Today Proc.* **33**, 5653–5658 (2020).
41. Thakur, R. K., Singh, K. K. & Ramkumar, J. Impact of nanoclay filler reinforcement on CFRP composite performance during abrasive water jet machining. *Mater. Manuf. Process.* **36**, 1264–1273 (2021).
42. Thakur, R. K. & Singh, K. K. Experimental investigation and optimization of abrasive water jet machining parameters on multi-walled carbon nanotube doped epoxy/carbon laminate. *Measurement* **164**, 108093 (2020).
43. Thakur, R. K., Singh, K. K. & Rawat, P. Evaluation of graphene nanoplatelets addition and machining methods on the hole quality and bearing strength of glass- and carbon-fiber-reinforced epoxy laminates. *J. Manuf. Process.* **115**, 137–155 (2024).
44. Thakur, R. K. & Singh, K. K. Evaluation of drilling characteristics to explore the effect of graphene nanoplatelets on glass fiber reinforced polymer composite. *Measurement* **219**, 113233 (2023).
45. Thakur, R. K. & Singh, K. K. Evaluation of hole quality to explore the influence of graphene nanoplatelets embedded in epoxy/carbon composite during abrasive water jet drilling. *J. Manuf. Process.* **85**, 569–583 (2023).
46. Singh, K. K. & Thakur, R. K. Experimental analysis on carbon nanotube embedded GFRP composites during AWJM. *Mater. Manuf. Process.* **37**, 210–222 (2022).
47. Wang, G., Qiao, S. F., Wang, G., Jiang, H. & Singh, J. Cutting depth of pile materials subjected to the abrasive waterjet and its prediction model. *Tunn. Undergr. Space Technol.* **124**, 104473 (2022).
48. Karakurt, I., Aydin, G. & Aydiner, K. An experimental study on the depth of cut of granite in abrasive waterjet cutting. *Mater. Manuf. Process.* **27**, 538–544 (2012).

Acknowledgements

This paper is funded by the Key R&D Program of Shandong Province, China (2022CXPT016, 2024CXPT063), the National Natural Science Foundation of China (52309134, 42272311), the China Postdoctoral Science Foundation (2023M742095), Shandong Provincial Natural Science Foundation (ZR2023QE266), the Special Fund for Central Guidance on Local Science and Technology Development (YDZX2023121).

Author contributions

JX, HY and CH conceived the research idea and conducted the simulations. CH, BiaoL, and BinL provided supervision and guidance throughout the study. HY, JQ, CH, JX, JW, and BinL contributed to the manuscript's writing. BinL and HY critically reviewed and revised the manuscript for intellectual content.

Declarations

Competing interests

The authors declare no competing interests.

Additional information

Correspondence and requests for materials should be addressed to B.L.

Reprints and permissions information is available at www.nature.com/reprints.

Publisher's note Springer Nature remains neutral with regard to jurisdictional claims in published maps and institutional affiliations.

Open Access This article is licensed under a Creative Commons Attribution-NonCommercial-NoDerivatives 4.0 International License, which permits any non-commercial use, sharing, distribution and reproduction in any medium or format, as long as you give appropriate credit to the original author(s) and the source, provide a link to the Creative Commons licence, and indicate if you modified the licensed material. You do not have permission under this licence to share adapted material derived from this article or parts of it. The images or other third party material in this article are included in the article's Creative Commons licence, unless indicated otherwise in a credit line to the material. If material is not included in the article's Creative Commons licence and your intended use is not permitted by statutory regulation or exceeds the permitted use, you will need to obtain permission directly from the copyright holder. To view a copy of this licence, visit <http://creativecommons.org/licenses/by-nc-nd/4.0/>.

© The Author(s) 2025